Ocean Systems Engineering, *Vol. 12, No. 4 (2022) 439-459*
https://doi.org/10.12989/ose.2022.12.4.439

Experimental studies of impact pressure on a vertical cylinder subjected to depth induced wave breaking

Vipin Chakkurunnipalliyalil[a], Panneer Selvam Rajamanickam[*] and Sannasiraj Annamalaisamy Sannasiraj[b]

Department of Ocean Engineering, IIT Madras, Chennai, India

(Received July 14, 2022, Revised November 30, 2022, Accepted December 5, 2022)

Abstract. This paper describes experimental studies of impact pressure generated by breaking regular waves in shallow water on a vertical cylinder. Experimental work was carried out in a shallow water flume using a 1:30 - scale model of a vertical rigid circular hollow cylinder with a diameter 0.2 m. This represents a monopile for shallow water offshore wind turbines, subjected to depth induced breaking regular waves of frequencies of 0.8 Hz. The experimental setup included a 1 in 10 sloping bed followed by horizontal bed with a constant 0.8 m water depth. To determine the breaking characteristics, plunging breaking waves were generated. Free surface elevations were recorded at different locations between the wave paddle to the cylinder. Wave impact pressures on the cylinder at a number of elevations along its height were measured under breaking regular waves. The depth-induced wave breaking characteristics, impact pressures, and wave run-up during impact for various cylinder locations are presented and discussed.

Keywords: breaking characteristics; depth induced wave breaking; impact pressure; monopile substructure; wave runup

1. Introduction

Renewable energies ensure the world's energy resources, that it is safe, and that it is less dependent on fossil fuels and do not pollute the environment. Nearshore and offshore wind energy extracted via wind turbines play a significant role in contributing a clean energy source to the community. Various types of substructures are designed to support these wind turbines. These structures are typically found in intermediate or shallow water, where they may be damaged by asymmetrical and extreme waves, such as breaking waves. In order to meet the nation's energy needs, marine renewable energy sources are crucial. For this reason, all energy extraction equipment and offshore wind turbine support structures must be able to withstand the harsh sea environment for many years. For optimising the design of offshore wind turbines (OWT) the hydrodynamic loads from breaking waves on OWT substructures has to be taken into account.

The foundation, substructure, and tower are the three main components of a fixed offshore wind

*Corresponding author, Professor, E-mail: pselvam@iitm.ac.in
[a]Professor, E-mail: sasraj@iitm.ac.in
[b]Ph.D. Student, E-mail: vipincp.iitm@gmail.com

http://www.techno-press.org/?journal=ose&subpage=7 ISSN: 2093-6702 (Print), 2093-677X (Online)

turbine and the foundation is embedded in the seabed and the substructure connects the foundation and tower. Monopile, Gravity-based, Jacket, and Tripod are some of the fixed foundation options for an OWT. Monopile is the most popular and easiest to design and construct of all the OWT substructure options, and it is also the most cost-effective for water depths up to 30 m. The construction is usually built of a steel material that is cylindrical in shape. These massive steel pipes, known as the XL monopole, have a diameter of 2.5 to 6.0 m, are 50-60 m in length, and weigh roughly 500 tonnes. However, on deeper sites, they can have a diameter of more than 8 m and weigh more than 800 tonnes. The OWT substructure is subjected to enormous hydrodynamic loads as a result of breaking wave impact pressure and these impact loads period acting on the structures are comparable to the structure's natural period. Furthermore, the pressure exerted by breaking waves are high and cause significant loads on structural elements, resulting in irreversible structural damage.

Several experimental and numerical studies in this area can be found in the literature. There have been many experimental studies on the hydrodynamic impact on cylinders. Swaragi *et al.* (1984) and Tanimoto *et al.* (1986) investigated the vertical distribution of the wave impact force on a vertical cylinder for nearly breaking waves. They concluded that the slamming force intensity is triangularly distributed for a vertical pile, with the maximum pressure imparted at 70% of the maximum free surface elevation. Chan and Melville (1989) experimentally investigated the structure's relative location to the onset of wave breaking, i.e., wave impact is more influential in determining the extent of the impact region and the magnitude of impact pressure. Wienke and Oumeraci (2005) studied the breaking wave impact force on a slender vertical pile as well as inclined, through large-scale experiments on a model scale, and they concluded that the impact force is strongly dependent on the distance between the location of the breaking wave and the cylinder. When the wave broke directly in front of the cylinder, it exerted the greatest impact force on it. Arntsen *et al*. (2013) conducted a detailed experimental and numerical investigation on breaking impact pressure on slender piles in a customised wave flume. He observed that when the plunging breaking wave hit the cylinder as a vertical wall of water, the slamming force value was higher. In a large-scale model (1:12) study on breaking wave kinematics, local pressures, and pressure on a tripod support structure, Hilderbrandt (2013) observed that the magnitude of wave impact pressures can be ten times of non-impact pressures. Manjula *et al.* (2015) experimentally investigated the response of vertical slender cylinder under breaking wave impact due to constant amplitude as well as constant steepness spectrum. Pressure and acceleration measurements were made under the incidence of breaking waves of different intensities varying from plunging to spilling. The maximum acceleration observed under severe plunging was found to be higher under constant amplitude spectrum while under constant steepness spectrum, the acceleration was maximum for moderate plunging even though the pressure was maximum for severe plunging event. Chellaa *et al.* (2016) studied breaking characteristics and wave impact pressure interaction with a slender vertical cylinder and compared experimentally measured data with numerical results using REEF 3D. Kammath *et al.* (2016) numerically investigated the breaking wave interaction with a vertical cylinder and the effect of breaker location. They found the maximum wave pressure occurs when the breaking wave tongue impacts the cylinder just below the wave crest in all the cases simulated, and the minimum wave pressure occurs when the wave breaks behind the cylinder. Several wave features such as the splashing on impact, the splitting and re-joining of the wave around the cylinder resulting in a chute-like jet formation were identified.

Many experimental and numerical studies have confirmed that when a breaking wave with a partially developed wave crest strikes a vertical cylinder, the maximum wave impact pressure occurs

(Chella *et al.* 2019, Ha *et al.*2020). Ha *et al*. (2020) conducted a series of model tests to investigate the characteristics of wave impact loads and the associated air bubble effects on a vertical circular cylinder with various pressure and force sensors installed in a 2D wave flume . The air bubble effects were investigated by analyzing the time histories of the impact forces and pressures, and the effects were related to the natural frequency and sensing area of the sensors. The air bubble effects were observed to increase as the breaking wave developed more at the position of the cylinder. Vested *et al.* (2020) experimentally studied regular wave loads on a vertical cylinder divided into four section, and measured wave kinematics using Particle Image Velocimetry (PIV) and with Laser Doppler Velocimetry (LDV). They reported good agreement with previously published data, especially for the decomposition of the total force into corresponding harmonics. Esandi *et al*. (2020) compared the wave loading from highly nonlinear non-breaking waves and spilling breaking waves on the cylindrical model using focussed wave groups. They observed that the spilling breaking waves generate significantly larger forces and the load is increased by resonant and impact excitation of high natural modes and by direct high frequency excitation. Zhu *et al.* (2022) investigated experimentally the distributions of maximum pressures for plunging and spilling breakers on a monopile for breaking regular and irregular waves. They observed that the distribution of maximum wave slamming pressure was affected by the water depth and bottom slope. The significant wave height and turbulence kinetic energy dissipation had significant effects on the wave slamming forces.

Wave run-up can also cause unexpected damage to offshore structures. Accurate prediction of wave run-up can both help reduce building costs and avoid the risk of wave impact and damage to the platform. In previous works, the focus has been on the horizontal forces, whereas the wave run-up has been studied in less detail. Kriebel (1998) research concentrated on the run-up for periodic waves on a flatbed. The results were compared to theories of first and second-order analytical wave diffraction. The 2nd order diffraction theory produced 50% more run-up than the 1st order theory, while the experiments produced values that were 83% higher than the 1st order theory. This shows that the non-linearity of the waves has a significant impact on the total run-up. Chan *et al.* (1995). investigated the run-up and, in particular, the impact pressure on a circular cylinder in the presence of a plunging breaker. According to the findings of that study, the breaking process has a significant impact on wave run-up. Büchmann *et al.* (1998) investigated run-up on a structure in the presence and absence of current using a second-order boundary integral method. The sloping bed in front of the foundation can significantly improve run-up for a small diameter foundation, as demonstrated by Mase *et al.* (2001). They devised analytical equations for the run-up that took into account wavelength, wave height, and slope. The diameter, however, was not included in their analytical expressions, despite the fact that basic diffraction theories show that the diameter has a fairly clear effect on the run-up. Jian *et al.* (2017) investigated experimentally the wave runup on a vertical cylinder surging in regular waves. They observed that the phase between the surge motion and incident wave has strong effect on the wave runup. An empirical equation was proposed for predicting the maximum runup ratio from known incident wave and surge conditions. Grue *et al.* (2020) studied runup on a vertical column due to breaking and non-breaking waves in deep water and finite water depth. Large water wave events were generated using focused wave techniques, and the wave runup speed and maximum runup on the slender column for various water depths were captured by a high-speed camera and digitised.

In order to evaluate the general behaviour of fixed OWT structures, hydrodynamic impacts on OWT substructures that are exposed to hostile sea conditions must be thoroughly examined. Significant errors are brought on by breaking waves when estimating extreme loads, life of structure due to cyclic loads, besides hydrodynamic loads. Compared to offshore oil and gas structures,

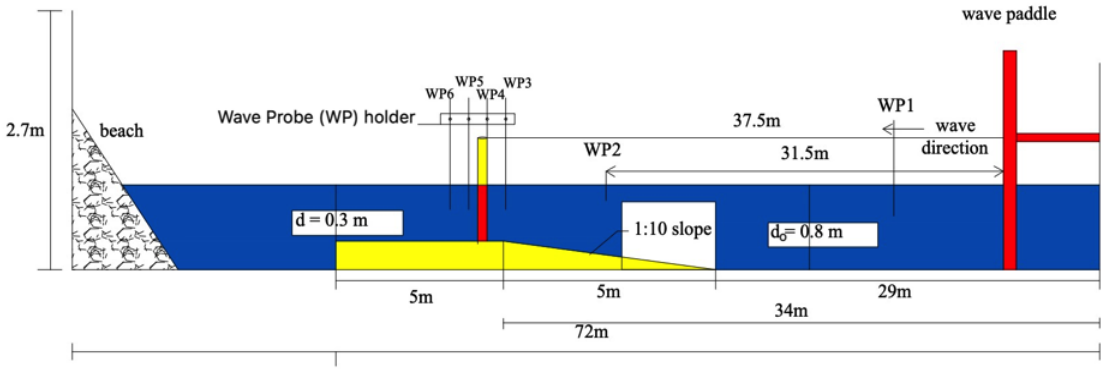

Fig. 1 Schematic diagram of the experimental setup in the wave flume

offshore wind turbine design loads are more susceptible to dynamic factors. The rules and design processes for offshore wind turbine substructures must therefore be carefully examined. The entire design of an OWT structure requires a full understanding of depth-induced wave breaking and the related nonlinear hydrodynamic loads on substructures. With today's state-of-the-art computational capabilities, numerical modelling of wave impact has gained significance in comprehending impact characteristics; however, experimental investigations always take precedence because they are conducted under well-controlled conditions. The reliability of experimental results is superior to numerical simulation and field measurements. Previous failures of vertical breakwaters in the European and Asian countries (United Kingdom, Japan, and Italy) indicated that analytical methods might not be reliable for impact-type loading situations (Oumeraci 1994). In addition, laboratory studies have revealed that impact pressure plays a significant role in the overall wave loading caused by breaking wave impact. The majority of the experimental studies concentrated on wave forces without taking into account shallow water effects or nonlinear wave loads from breaking waves. An unexplored research area is an investigation of a depth-induced shallow water wave breaking characteristic and the hydrodynamic load caused by extreme breaking waves acting on a fixed OWT substructure in a shore area. The primary objective of the ongoing research is to gain an experimental understanding of the kinematics of incident waves as well as the structural and hydrodynamic responses caused by breaking wave impact. This paper describes the details of experiments involving the generation of depth-induced breaking waves, the measurement of impact pressures due to different breaking waves to determine the maximum intensity of breaking on an instrumented vertical cylinder, the measurement of pressure at various locations above and below still water level on the instrumented vertical cylinder and the measurement of the run-up for maximum intensity of breaking.

2. Experimental setup

Elaborate experimental studies were conducted in the shallow water wave flume at the Department of Ocean Engineering, Indian Institute of Technology Madras, India. The flume is 72 m long, 2 m wide and 2.7 m deep. Tests can be conducted for varying water depths in the range of 0.3 m to 2 m. Fig. 1 depicts a schematic view of the experimental setup in the flume. At the far end of

Table 1 Wave Probe locations

Wave probe	Distance from paddle (m)	Location
WP1	5	At 80 cm water depth near the paddle
WP2	31.5	Half way down the slope
WP3	34.2	At the flat bed before wave breaking
WP4	34.5	At wave breaking point
WP5	34.7	Just after wave breaking(Post breaking)
WP6	34.9	At broken wave

the flume, there is also an artificial beach with a reflection coefficient of about 0.05. To generate waves, the wavemaker is outfitted with a piston. At a distance of 29 m from the wave paddle, a ramp of 1 in 10 slope was built to generate depth-induced breaking waves.

The water depth in front of the ramp was kept as 0.8 m. The sloping ramp was built for 5 m length to achieve a maximum depth variation from 0 to 0.5 m, followed by a 5 m constant section. As a result, a water depth of 0.3 m behind the slope was maintained as shown in Fig. 1. Plywood boards were used for fabricating the submerged ramp. The plywoods were securely fastened to steel frames, and bolted to the flume walls and floor. The plywood board's surface was painted to achieve a smooth bottom and better visibility. Six wave probes (WP1 to WP6) were used during the tests to measure the free surface elevation at various locations. WP1 was positioned ahead of the ramp at a water depth (d_0) of 0.8 m at 5 m in front of the paddle, and WP2 was positioned halfway down the ramp in a water depth of 0.50 m to record shoaling free surface elevation. Four-wave probes were fixed using a single rigid frame with 0.25 m spacing along the wave flume in the wave breaking zone near the cylinder. To determine the wave breaking properties, the wave probes, WP3 and WP4 were positioned at the wave breaking zone at 34.2 and 34.5 cm, respectively from the wave paddle. To determine the post-breaking wave characteristics, WP5 and WP6 were positioned at 34.7 m and 34.9 m, respectively. Table 1 shows the relative positions of wave probe from wave paddle. Two run up probes, WP7 and WP8, were attached to the front face and side of the vertical cylinder, respectively, to measure the run up of the breaking wave. Without the model, the breaking wave was traced along the wave flume at various positions within the breaking region and the breaking wave simulation was tested for repeatability.

2.1 Depth induced wave breaking generation

Before positioning the cylinder, it was critical to determine the wave height and time period of the regular waves generated by the paddle so that the waves would undergo depth-induced breaking just after the ramp. During the propagation of waves over a slope, the water depth changes, resulting in a reduction in wave velocity, or wave motion. Increased wave heights result from a shorter wavelength (L) and a constant wave period (T). The local wave steepness increases as the wave propagate into shallow water and it attains the maximum value at the breaking point. Considering the nonlinear behaviour of shallow-water waves, the shortening of wavelength leads to larger wave heights. The steep slope of the seabed has significant influences on the development of the free surface during the shoaling and breaking process. These influences are in addition to the strong wave-wave interaction that is present. A schematic sketch of depth-induced wave breaking is shown

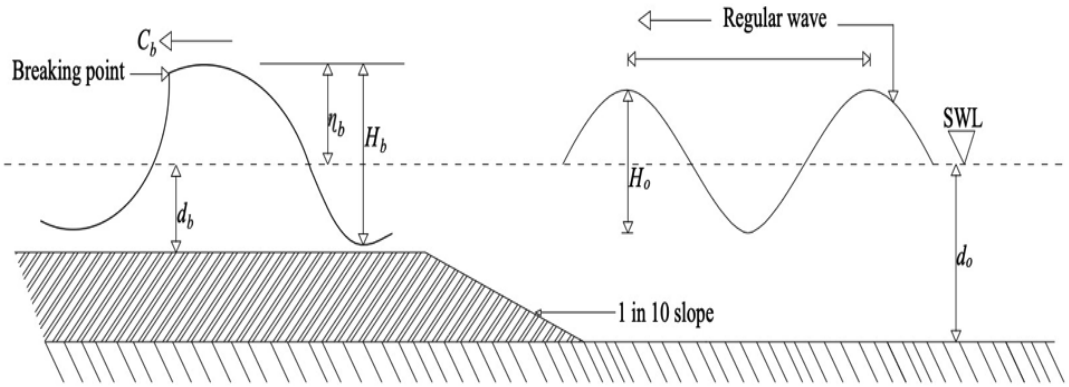

Fig. 2 Wave profile of breaking wave

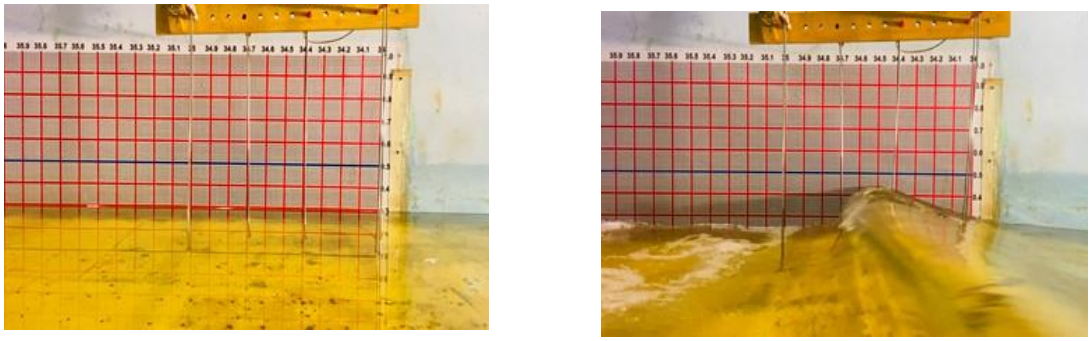

(a) Side view of breaking zone with mesh scale fixed on the wall

(b) Side view of breaking zone during breaking waves

Fig. 3 Snapshot of breaking zone

in Fig. 2. It shows the breaking wave profile *(η_b)* characterized by the breaking wave height *(H_b),* water depth *(d)* and celerity *(C_b)* at breaking.

As the wave propagates over the slope from intermediate to shallow water, the depth limited breaking criterion describes the wave breaking through wave height (*H*) and water depth (*d*). The water depth starts reducing as waves propagate over the slope and the waves start breaking when the ratio of *H/d* reaches 0.8 and above, also taking the shallow water wave criterion (*d/L*< 0.05) into account, waves with time periods ranging from 1.3 s to 1.57 s and wave heights ranging from 18.6 cm to 22.8 cm were chosen. Within this limit and the number of trial runs, a total of eight cases were selected for the study. The details of wave inputs and breaking points for these eight different cases are given in Table 2. The efficiency of the wave absorber in terms of wave reflection is more than 94% for the non-breaking waves. To achieve a stable wave before the slope, the ramp was placed 12*L* away from the wave paddle, where *L* is the wavelength for the maximum wave period. Further, a sufficient distance (more than15*L*) was provided behind the slope and the flume end wall to reduce the influence of reflected waves. A measuring scale of 5 m length was pasted on the sidewall of the

Table 2 Wave inputs and breaking parameters

	Wave period(s)	Incident wave height (WP1)H_0 (m)	Wave breaking height (WP4) H_b (m)	Wave breaking point from paddle L_b (m)
Case 1	1.3	0.186	0.2318	35.2
Case 2	1.4	0.204	0.2492	35.2
Case 3	1.43	0.210	0.2618	35
Case 4	1.47	0.216	0.2708	34.7
Case 5	1.50	0.222	0.2806	34.6
Case 6	1.52	0.228	0.3012	34.5
Case7	1.55	0.228	0.3001	34.3
Case 8	1.57	0.228	0.2956	34.5

Table 3 Breaking characteristics

Case	η_b(m)	H_b(m)	$\Omega_b = H_b/H_0$	$\gamma_b = H_b/d$	$\mu_b=\eta_b/H_b$	C_b(m/s)
1	0.1703	0.2318	1.136	0.772667	0.704	2.033
2	0.1867	0.2492	1.221	0.830667	0.703	2.075
3	0.1958	0.2618	1.24	0.872667	0.704	2.09
4	0.1978	0.2708	1.253	0.902667	0.704	2.10
5	0.2032	0.2806	1.263	0.935333	0.704	2.09
6	0.2121	0.3012	1.321	1.004	0.704	2.124
7	0.2113	0.3001	1.316	1.000333	0.704	2.123
8	0.2081	0.2956	1.296	0.985333	0.704	2.118

flume from 34 m to 39 m to track wave breaking profile in the wave breaking zone. This scale helps to spot the wave breaking point and to fix the wave probes at a different location to trace the free surface elevation at breaking zone. The side view of the breaking zone with a mesh scale of a range of 1 cm pasted on the flume is shown in Fig. 3. Fig. 3(a) shows the snapshot of the mesh scale fixed on the wall and Fig. 3(b) shows the snapshot during the breaking wave. Three cameras were installed at different viewpoints: one from the wavemaker end, one perpendicular to the wave direction, and one from the beachside. η_b, L_b and H_b, were recorded using video cameras. The time duration for each run was set to 95 seconds; within this duration total of 60 waves were generated by the paddle, and it was observed that the first 35 to 45 waves were identical and broke at the same fixed point. However, due to reflection from the wave absorber and the slope's reflection effect, subsequent waves broke a little earlier and their intensity was reduced. In order to measure the pressure and overall wave forces, the first 30 waves were considered in this study.

For each case of wave generation, the free surface elevation (η_b) and breaking wave height (H_b) were measured as the wave propagated down the slope.WP4 was placed at the wave breaking point in each case to measure (H_b) and (η_b), video cameras facing the wave breaking zone gave the breaking point on the measuring scale pasted on the wall. As the incident wave propagate over the slope, the wave crest increases to 1.85 times and the wave height at breaking increases to 1.32 times due to shoaling. As the particle velocity at the wave crest exceeds the wave celerity, the wave crest

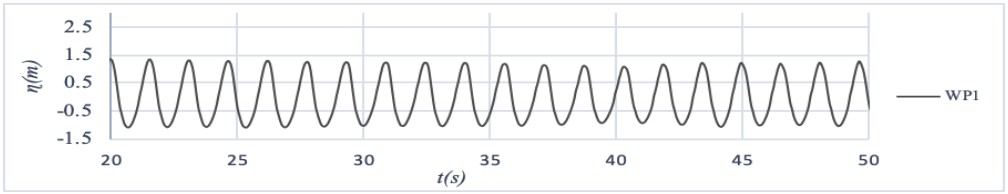

(a)

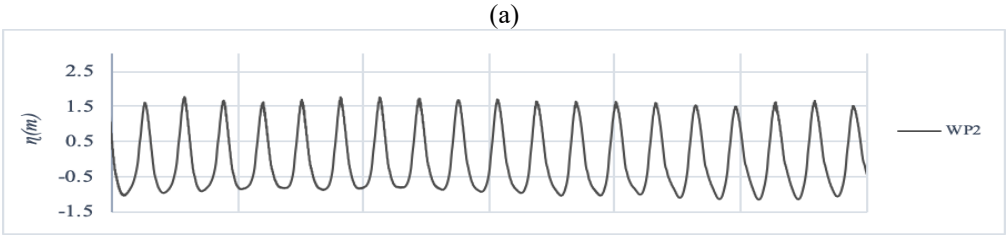

(b)

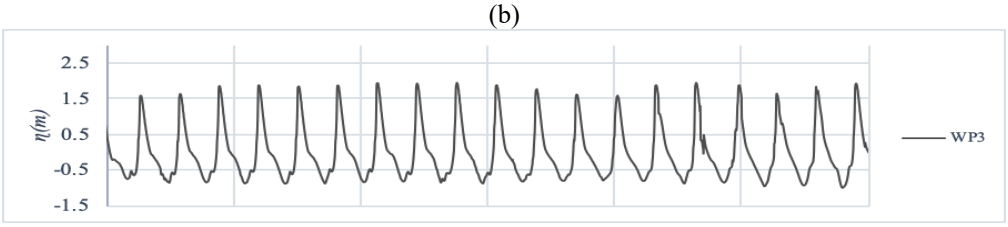

(c)

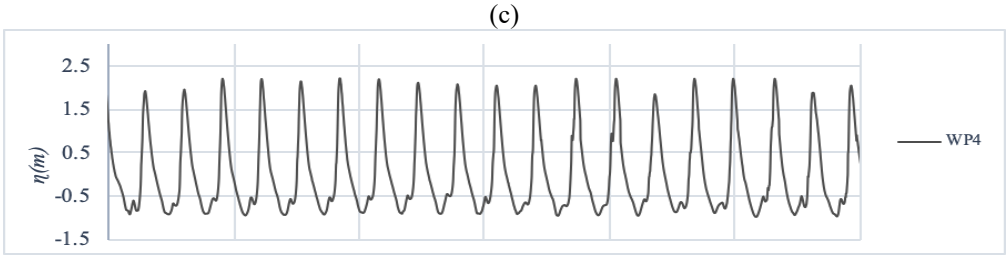

(d)

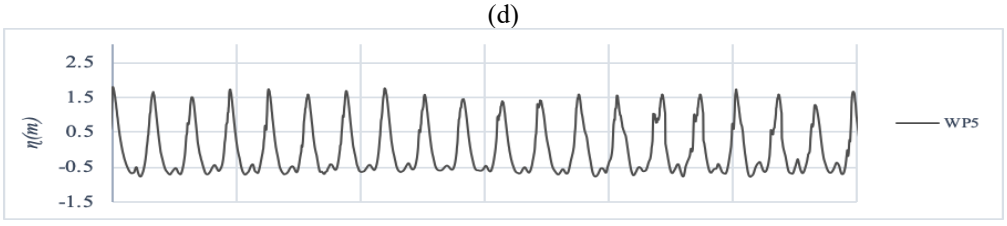

(e)

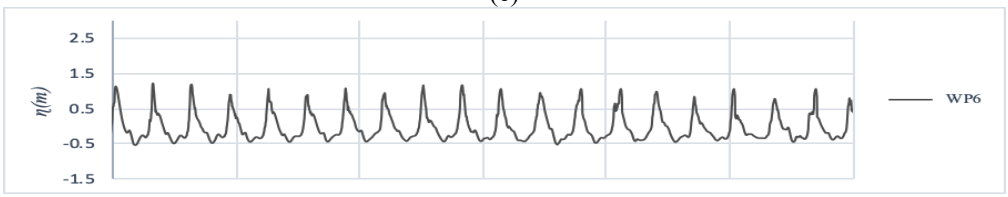

(f)

Fig. 4 Measured free surface elevations at all the wave probe locations for Case 6

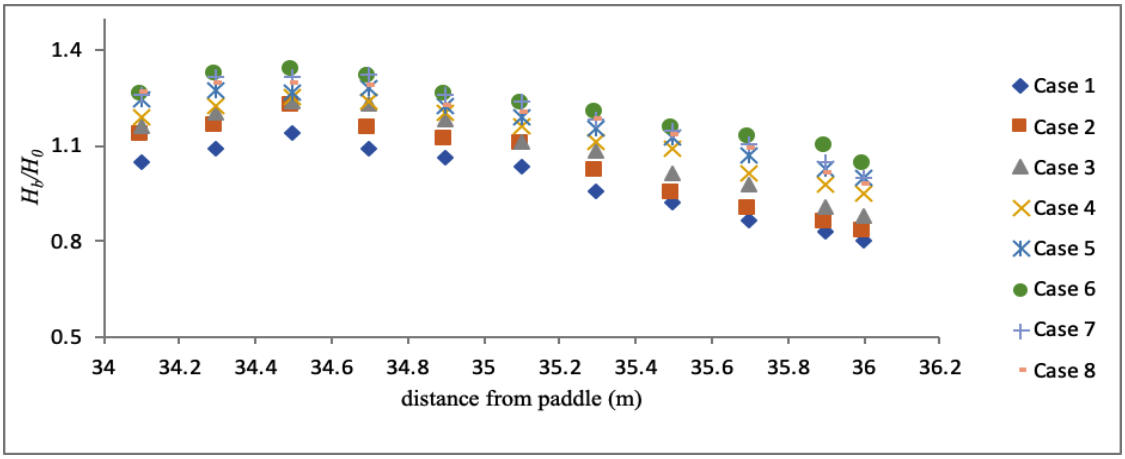

Fig. 5 Variation of breaker height index on the wave breaking zone

moves faster than the rest of the wave resulting in plunging waves. As a result, predicting the wave celerity at breaking is critical for estimating the breaking wave force, Wave celerity ($C= L/T$) is calculated from the wave gauge measurements in the absence of the cylinder model, where L denotes the wavelength and T denotes the period between the preceding and primary crest of breaking wave. For all eight cases, the wave height increases and the wave profile shape becomes steeper as the waves propagate over the slope due to shoaling. The incident wave characteristics change significantly and the wave crest becomes more asymmetric. Breaking waves are distinguished by their height and water depth at breaking and breaker types, which are used to describe the maximum hydrodynamic pressure on coastal structures. Breaking wave characteristics are listed in Table 3 namely horizontal asymmetry factor ($\mu_b = \eta_b /H_b$), and the breaking wave celerity (C_b) for all the eight cases. From Table 3, it can be observed that the maximum and minimum free surface elevations appear for Case 6 and Case 1, respectively.

Ω_b represents the strength of wave breaking and is used as the breaking intensity parameter for all input wave situations. At 34.5 m from the wave paddle, Case 6 exhibits the most significant breaker height index and the breaking point for Case 6 is known as the wave breaking hotspot because it will produce maximum impact on the structure. The different free surface elevations recorded by wave gauges for Case 6 are shown in Fig. 4. Free surface elevation near the wave maker and the half way slope from WP1 and WP2 are shown in Figs. 4(a) and 4(b) respectively. WP3 was placed at the end of slope gives the shallow water profile as shown in Fig. 4(c). WP4 gives the breaking height (H_b) at 34.5 m from wave paddle as shown in Fig. 4(d). Finally two wave probes are pinned after the breaking to examine the post breaking characteristics as shown in Figs. 4(e) and 4(f). The model cylinder was placed in the wave breaking zone for this case and the impact pressure and run-up measurement on the cylinder are the subjects of this research, as well. The variation in breaker height index for all eight wave cases on the wave breaking zone is shown in Fig. 5.

2.2 Instrumented cylinder

Steel pipe with a diameter of 0.2 m and a thickness of 0.0055 m was used to create a 1:30 scaled cylinder model. The cylinder was 1 m long, with a base plate at the bottom and a stiff box frame constructed of four angle sections at the top, which was supported to the flume's surface. The

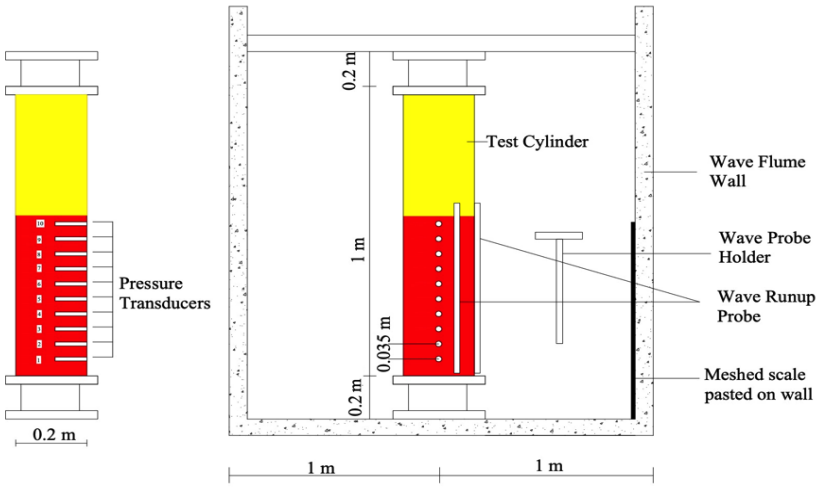

Fig. 6 Details of the instrumented cylinder

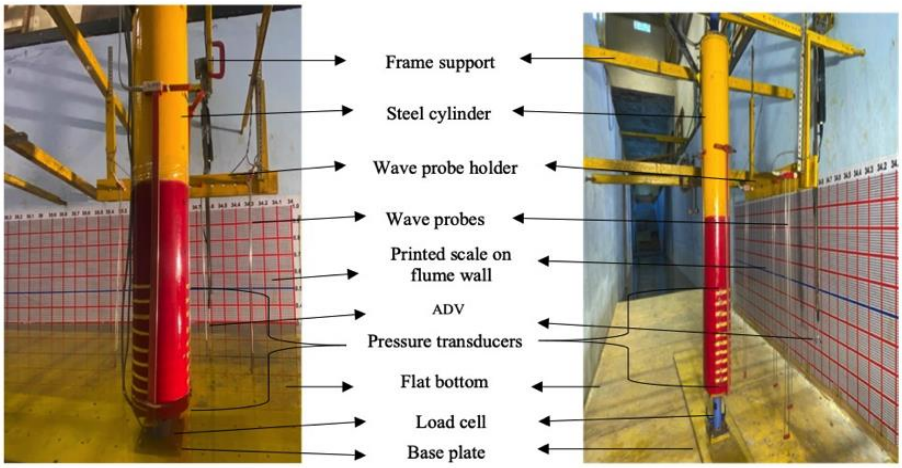

Fig. 7 Snapshot of physical scaled model of the instrumented cylinder on the ramp in the wave flume

cylindrical model was tightly fastened in the middle of four angles using a metal cover that was about 4 cm in length. The top and bottom side movements have been completely eliminated by proper fixity. The cylindrical model was completely sealed to ensure that it was watertight. The cylinder was positioned in the centre of the 2 m wide flume. Fig. 6 shows the details of fixed instrumented cylinder model at the breaking zone. Kistler industrial usage flush type diaphragm pressure transducers with a range of 0.5 bar were used to measure the induced pressure on the cylinder. Pressure transducers were screwed into the steel cylinder pipe from the inside, with the flat front face aligned with the cylinder's outside surface, as illustrated in Fig. 6.

The wave impacts the diaphragm of the pressure transducers linked along the front face of the cylinder in a tangential direction to the cylinder surface. The wave-induced dynamic pressures were measured using ten transducers placed vertically along the cylinder at ten different heights. The

Fig. 8 A snapshot of the test run in the wave flume for Case 6

pressure sensors were uniformly positioned at 0.035 m intervals. To measure the in-phase wave height and wave run up, two wave probes were kept parallel to the front face of the vertical cylinder.

Snapshot of physical scaled model of the instrumented cylinder in the wave flume showing the pressure measurement positions along the length of the cylinder is shown in Fig. 7.

3.Results and discussion

3.1 Pressure measurement with cylinder at the breaking point

The cylinder was placed at 34.5 m from the paddle where the maximum intensity of breaking wave was observed for Case 6. Temporal variation of pressure on the vertical cylinder was measured during the impact for all the waves. A snapshot taken during the experiment is shown in Fig. 8. A 16-bit HBM data acquisition system was used to sample the pressure data at a rate of 20 kHz. The run tests were sampled with a recording frequency of 20 kHz. The fifth pressure transducer (PT5) is located at the height of 0.07 m from the SWL and provides the maximum pressure. The fourth (PT 4) and sixth (PT6) transducers, placed at 0.035 cm and 0.105 cm from SWL, respectively, respond next. Fig. 9 depicts the measured response of twenty breaking waves hitting on PT5 for Case 6. The peaks in the image reflect each breaking wave impact on the cylinder. The peaks are observed to be considerably diverse among them. They do have different values for each transducer. As can be seen in Fig. 9 they also have a lot of variabilities even within the same transducer measurement. Because many factors affect the waves, the pressure on the cylinder for all of the waves in the same case is not equal. There are numerous reasons why a wave paddle cannot produce identical waves. The transducer reacts very differently to even slight variations in wave height. Another factor is wavefront inclination; in general, a wavefront that strikes a cylinder vertically produces a stronger response because it makes the most surface contact with the pressure transducer's diaphragm. Also of interest is the breaking position. According to Wienke and Oumeraci (2005), the wave breaks directly in front of the cylinder when it exerts the most force. Another factor to consider is the wave reflection at the wave flume's end. It is also important that the pressure intensity at each pressure transducer along the vertical cylinder confronting the breaking waves are compared. Below SWL,

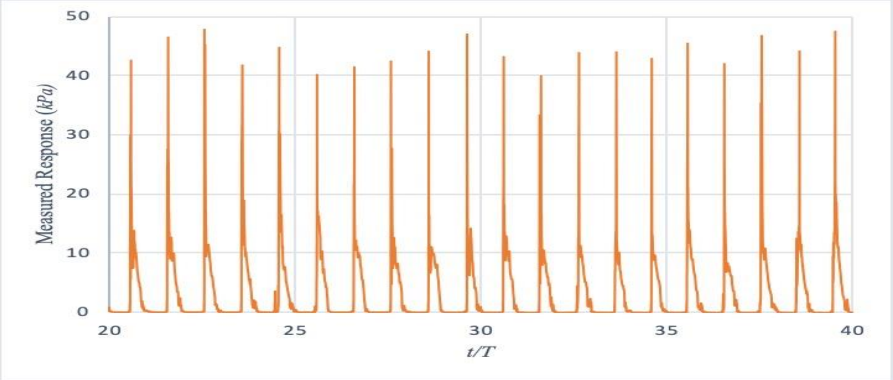

Fig. 9 Wave impact pressure on PT5 versus normalized time (t/T) for Case 6

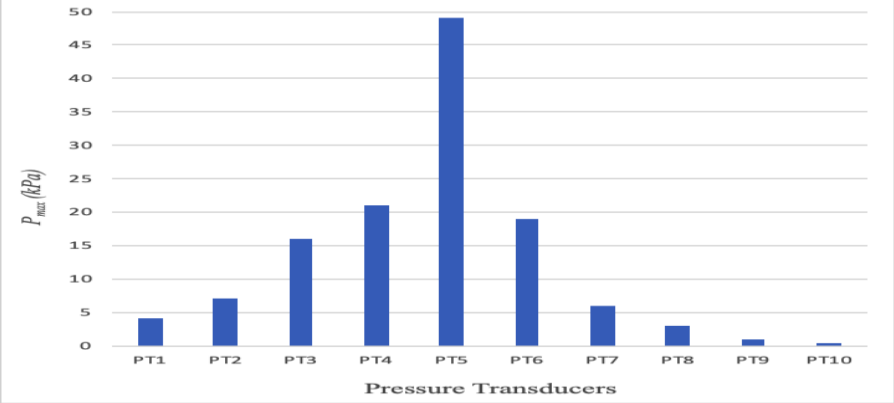

Fig. 10 Maximum impact pressure(P_{max}) acting on the pressure transducers from 20 runs of Case 6

static component of pressure also contribute to the dynamic component of pressure and there is no hydrostatic pressure when the wave crest strikes the cylinder (above SWL). A stacked chart showing the maximum response of all ten pressure transducers from 20 runs of Case 6 is shown in Fig. 10. Case 6 were repeated for 20 times for repeatability and the maximum impact pressure acting on the pressure transducers (p_{max}) was selected from the impact pressure data of all the waves hitting on it. Maximum impact was observed high on PT5 in every run and it was two times higher than the following maximum impact observed on PT4 and PT6 respectively.

3.2 Pressure measurement with cylinder at different locations with respect to breaking point

The cylinder was shifted to different locations with respect to the breaking point in order to get different stages of impact of the breaking wave. Depending on the distance between the concentration point (breaking location) and the wave paddle, the cylinder was moved in either direction. A total of five test series were performed, each with a different cylinder location based on the distance between the breaking location and the cylinder as shown in Fig. 11. The five cases are referred to as Case L1, Case L2, Case L3, Case L4, and Case L5. The location of the breaking point

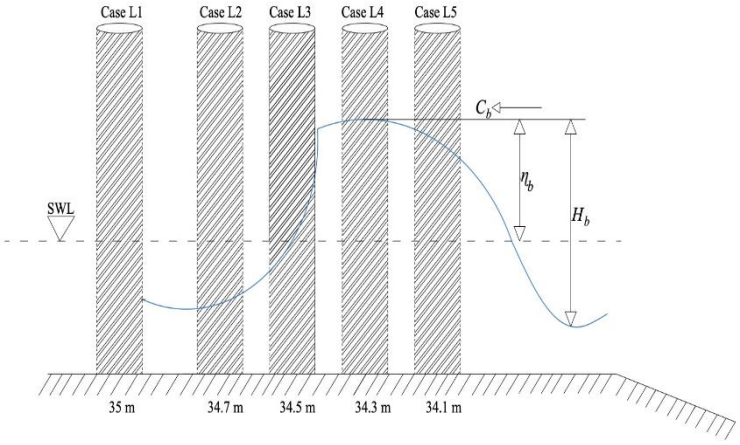

Fig. 11 Schematic representation of different cases of the cylinder location considered for the study

is represented by L3 (34.5 m). L1 and L2 indicate the cylinder's locations after breaking at 35 and 34.7 metres, respectively, and L4 and L5 represent the cylinders' locations before breaking at 34.3 and 34.1 metres, respectively.

Fig. 12 depicts snapshots of cylinder and wave profile at these five-cylinder locations. Wave probes were unable to accurately identify the breaking position, and visual aids proved to be the most reliable method of determining the distance between the breaking spot and the cylinder (video record). The wave characteristics are varying at different cylinder locations with respect to the breaking point (Case L3). For all the five-cylinder locations; height index (H_r/H_o), depth index (H_r/d) and wave celerity (C_r) were measured and are presented in Table 4, where H_r and C_r are the wave height and wave celerity at the given point. The overall pressure and the point of maximal impact on the cylinder differ for each cylinder location. The cylinder experienced the greatest impact force when the wave broke directly in front of it. It was observed when the cylinder was placed at 34.5 m from the paddle. In this case, the wave crest hits the cylinder at a greater elevation than the other test cases.

At each cylinder locations, Case 6 was repeated for 20 times for repeatability and the maximum impact pressure (p_{max}) of breaking wave hitting on each pressure transducers were recorded. Free surface elevation (η_b), wave breaking point (L_b) and breaking wave height (H_b), were recorded using video cameras. The maximum impact pressure acting on the pressure transducers (P_{max}) was selected from the impact pressure data of all the waves hitting on it. P_{max} is normalized with ρC_b^2 (where ρ is the density of water (=1000 kg/m^3) and C_b (m/s) is the wave celerity at breaking). The variation of normalised maximum impact pressure $P_{max}/\ \rho C_b^2$ along the height of the cylinder from top to bottom are depicted for the five loading instance in Fig. 13. The vertical elevation (z) is normalized with (η_b), i.e., normalized to one at the top of the wave crest and zero at the still water level. The maximum impact was observed at 0.07m (z/η_b =+0.33) above SWL at fifth pressure transducer (PT5) for Case L3 followed by Case L2 (PT3) and case L4(PT6) at 0.035 m and 0.105 m from SWL respectively. Below SWL, the pressure variation is almost uniform for all cases except Case L5 (non breaking wave).

(a) Case L1

(b) Case L2

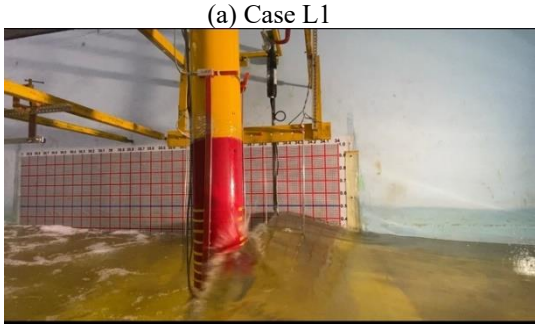

(c) Case L3

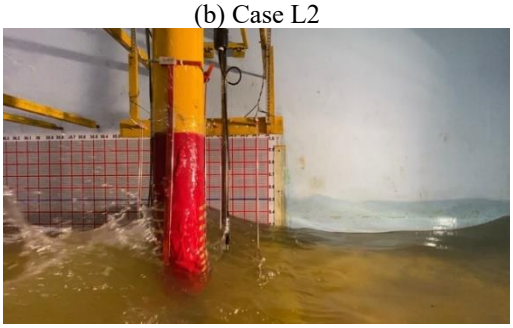

(d) Case L4

(e) Case L5

Fig. 12 Snapshot showing the details of breaking (breaker tongue) near the cylinder for Case L1, Case L2, Case L3,Case L4 and Case L5

In Tables 5 and 6, a comprehensive comparison of wave breaking characteristics and maximum impact pressure obtained from other studies with either a flume with a flatbed bottom or a bed slope (depth-induced wave breaking) is presented. In addition to comparing the maximum impact of the breaking wave on the cylinder, the features of the experimental setup, such as the diameter of the test model, wave velocity, and wave crest elevation, were analysed. In Table 5, there is a substantial variation in the impact pressure values $(P_{max}/\ \rho C_b^2)$ for the studies without a bottom slope. Large-scale experiments(1:12) conducted by Wienke and Oumeraci (2005) with bigger flume size and cylinder diameter showed the greatest impact (10 times larger impact). The discrepancy was linked to the process of generating the diving breaker artificially using Gaussian wave packets and not to the large scale. In this case, the wave breaking pattern will differ from waves breaking due to bottom constraints. The difference may also be attributed to the existence of entrained air at the impact, which causes the breaker to strike the cylinder with a greater force. Due to the compressibility effect,

Table 4 Characteristics of five-cylinder location Cases

Location Cases.	Characteristics
Case L1 • Distance from the paddle 35 m • Cylinder was placed far from the wave breaking point • A broken wave hitting the cylinder	• Height index (H_r/H_o)= 1.12 • Depth index (H_r/d)=0.95 • wave celerity C_r=1.57
Case L2 • Distance from the paddle 34.7 m • Cylinder was placed in front of the wave breaking point • A strongly breaking wave hitting the cylinder	• Height index (H_r/H_o)=1.17 • Depth index (H_r/d) =0.96 • wave celerity C_r=1.96
Case L3 • Distance from the paddle 34.5 m • Cylinder face at wave breaking point • Breaking wave hitting the cylinder (impact wave)	• Height index (H_b/H_o)=1.321 • Depth index (H_b/d)=1.004 • wave celerity C_b=2.24
Case L4 • Distance from the paddle 34.3 m • Cylinder before the wave breaking point • No wave breaking in front of the cylinder • Partially breaking waves hitting the cylinder	• Height index (H_r/H_o)=1.11 • Depth index (H_r/d)=0.89 • wave celerity C_r=*1.98*
Case L5 • Distance from the paddle 34.1 m • Cylinder was placed ahead of the wave breaking • No wave breaking in front of and at the cylinder • Non breaking wave	• Height index (H_r/H_o)=1.14 • Depth index (H_r/d)=0.97 • wave celerity C_r=1.78

the influence of even a little amount of air entrained in water is significant. Air can be entrained in water either as microscopic bubbles or as a pocket of air.

In Table 6, tests with bottom slope, the horizontal asymmetry factor remains nearly constant in each study despite variations in breaking wave surface elevation, water depth, and breaking wave height. Impact pressure $(P_{max}/\ \rho C_b^2)$ observed in the present study is comparable to prior investigations and shows a good correlation with wave breaking characteristics. Due to the placement of the cylinder on the slope, the present study with a bottom slope of 1:10 produces breaking waves with a greater plunging effect than previous experiments. In Sawaragi and Nochino (1984) and Tanimoto *et al.* (1986), the cylinder was placed in the transition zone between the flat zone and the slope. However, in the current investigation, the cylinder was placed on the flat bottom, i.e., after the slope terminates. Consequently, the differences in wave breaking pattern, air entrapment, and the inclination of the pile's placement bottom are the primary causes for the difference in impact force between sloped and non-sloped conditions.

Table 5 Previous studies of breaking wave impact on vertical fixed cylinders (Without bed slope)

Study	Cylinder Dia(m)	η_b(m)	η_b / H_b	Wave Celerity C_b(m/s)	Bed Slope	Maximum Impact Pressure $(P_{max}/\ \rho C_b^2)$
Chan *et al.* (1995)	0.216	0.185	0.72	1.9323	0	14
Wienke and Oumeraci (2005)	0.70	2.0	0.71	6	0	25
Manjula *et al.* (2015)	0.20	0.197	0.72	2.053	0	11.3
Ha *et al.* (2020)	0.3	0.16	0.7	1.967	0	18

Table 6 Previous studies of breaking wave impact on vertical fixed cylinders (depth induced wave breaking)

Study	Cylinder Dia(m)	η_b(m)	η_b / H_b	Wave Celerity C_b(m/s)	Bed Slope	Maximum Impact Pressure $(P_{max}/\ \boldsymbol{\rho C_b^2})$
Sawaragi and Nochino (1984)	0.07	0.097	0.8	1.8	1/30 and 1/15	14
Tanimoto *et al.* (1986)	0.14	0.195	0.75	1.97	1/30 and 1/100	10
Arntsen *et al.* (2013)	0.06	0.21	0.72	2.3	1/30,1/15	12
Present study	0.20	0.2121	0.704	2.124	1/10	11.7

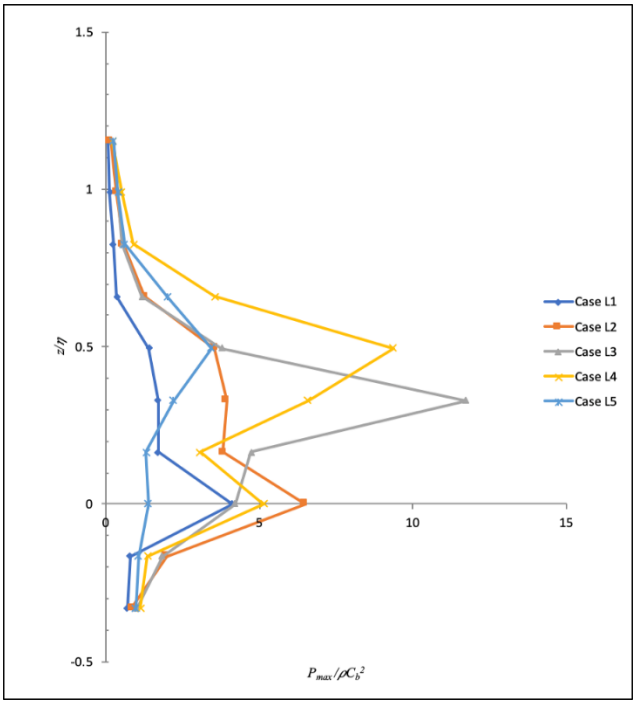

Fig. 13 Pressure variation along the cylinder's elevation caused by breaking waves of varying intensities

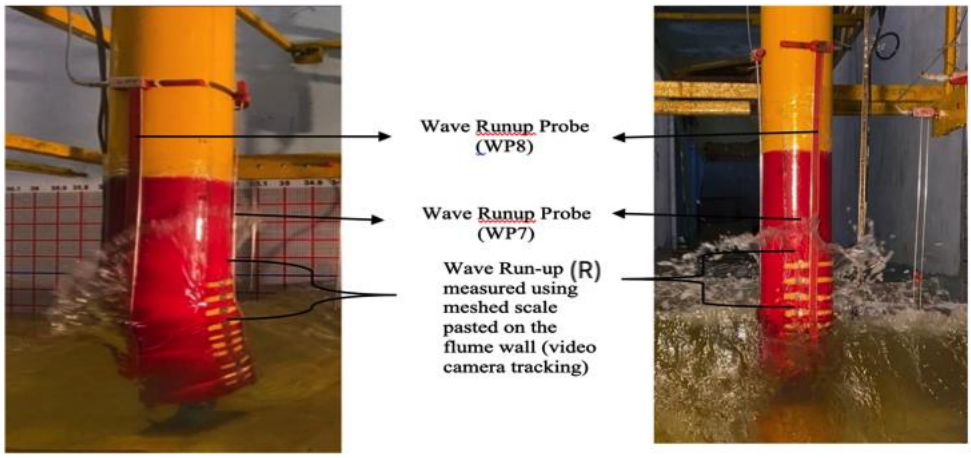

Fig. 14 Snapshots of the measurements of run-up on the cylinder for a typical test run

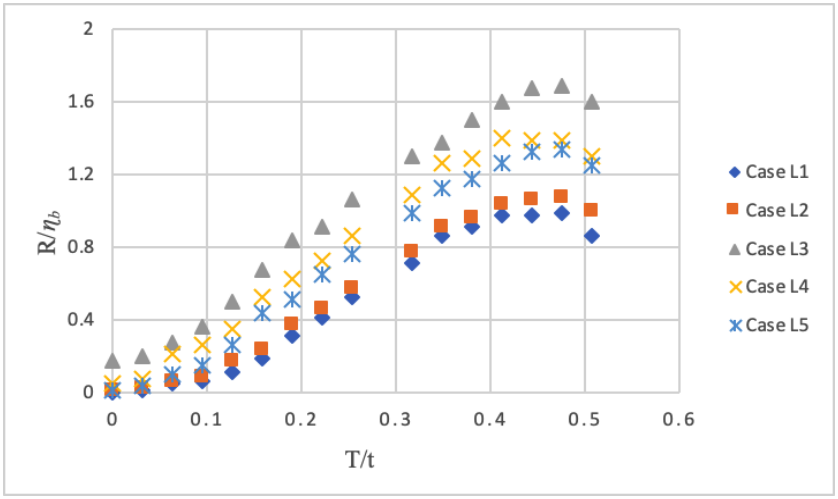

Fig. 15 Wave run-up vs normalized time for five-cylinder positions

3.3 Wave run-up on the cylinder

In wave-structure interaction, the Wave run-up (R) is an important phenomenon that needs to be considered in the design of offshore structures. When a wave hits on a coastal structure the maximum vertical distance of the wave uprush on the structure above the still water level (SWL) is called R. Fig. 14 shows the snapshots of run-up measurement on the cylinder using the run-up wave probes and meshed scale pasted on the flume wall. This vertical water motion caused by the wave-body interaction may cause local damage to the structure. Previous works on the effect of breaking waves on run-up have received a lot of attention. Along with the pressure measurements, run-up on the vertical cylinders was studied by varying the cylinder location with respect to the breaking point for Case 6 during the highest intensity of breaking wave incidence. Video camera records the breaking process and the meshed scale pasted on the sidewall of the flume traces the wave run-up on the

Table 7 Comparison of present study with Grue *et al.* (2017)

	h/D	$\eta_b(m)$	D/d	R/η_b	Breaking at
Grue *et al*. (2017)	2.5	0.951	0.567	1.97	Infront of cylinder
Present Study	1.5	0.2121	0.667	1.85	Infront of cylinder

cylinder. The constants for this study are D/d = 0.667 and H_0/d = 0.76, where D is cylinder diameter, d is the shallow water depth and H_0 is the deep-water wave height. The run-up at five different cylinder locations is compared. Wave run-up, R is measured at each cylinder location, the run-up is made dimensionless with breaking wave height H_b and dimensionless wave run-up (R/H_b) is plotted against normalized time (t/T) in Fig. 15, where t is the rise up time for wave run-up from 0 to maximum and T is the wave period. When the cylinder position is changed from Case L1 to Case L3, the run-up increases by 33% for the dimensionless wave height, H_0/H_b of 0.667. When the cylinder position is changed from Case L5 to Case L3, the run-up increases by about 10% to 15%. When the cylinder goes from Case L4 to Case L3, the run-up appears to be high. This indicates that the maximum run-up occurs just before the wave breaks. It is found that the maximum R/H_b is varying with respect to the cylinder location cases in the range of 0.9 to 1.7 as shown in Fig. 15. The maximum and minimum run-up was observed for case L3 and case L1 respectively. This shows that when the wave is just about to break, the run-up is higher than when the wave has fully broken. Several factors, such as the distance from the slope to the vertical cylinder, the influence of irregular waves in the whole three-dimensional sea, and a varied foundation form, should also be considered.

The present experimental results are compared with those obtained by Grue *et al.* (2017). They measured the run-up for an 8 cm vertical column with non-breaking and breaking waves of finite depth. Focusing wave approaches were used to generate breaking wave occurrences for intermediate and shallow water, and a typical case with H/d = 2.5 was compared to the current study. Table 7 compares the nondimensional wave runup and breaking characteristics with the present investigation. Maximum runup was seen in both trials when the wave broke in front of the cylinder, as indicated in the Table 7, and the runup of a breaking wave depends on the cylinder diameter (D), water depth (d), and the location of the breaker (L_b). The non-dimensional runup (r/ η_b) shows good match with the present study even though the breaking wave surface elevation (η_b), water depth and cylinder size vary.

3.4 Run-up pressure on cylinder

The run-up has been shown to have significant effects on impact pressure acting on the vertical cylinder. The characteristics of wave run-up and consequent dynamic wave pressure on the vertical cylinder are investigated for the five-cylinder locations. The run up pressure were measured using the last three pressure transducers fixed at the top of the cylinder which is above the maximum wave breaking surface elevation of 21 cm from the SWL i.e., PT8, PT9 and PT10 at 21, 24.5 and 28 cm from SWL respectively. The run-up is different in each scenario, and the pressure due to run-up is distinct as well. Wave run up, R is measured at each cylinder location, and dimensionless wave run-up (R/H_b) is plotted against normalized average (20 waves) run-up pressure in Fig. 16. It is observed that the breaking pattern, in addition to reflection from the vertical cylinder, increases the maximum crest wave elevation and wave pressure. Case L3 shows maximum run-up pressure which is 25% higher than Case L3 and Case L5. Minimum run-up pressure was observed for cases L1 and L2. The

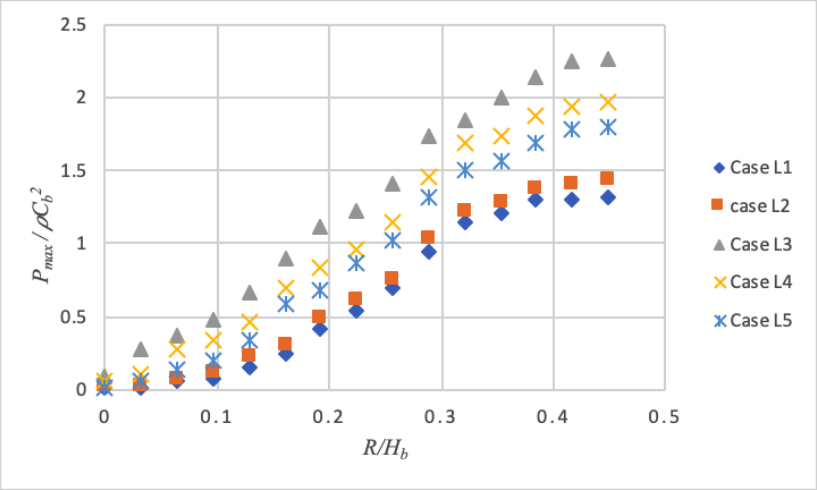

Fig. 16 Wave run-up vs pressure for five-cylinder positions

maximum wave run-up pressure on the vertical cylinder is 15 to 20% of the maximum pressure due to the breaking impact.

4. Conclusions

The depth-induced wave breaking induced impact pressure on a monopile substructure has been investigated experimentally. The characteristics of depth induced shallow water wave breaking due to a high steep bottom slope were studied and the temporal variation of pressure along the vertical face of the cylinder was carried out for the maximum intensity of breaking. The vertical distribution of peak values of the impact pressure were not evenly distributed over the cylinder's height and depends on wave breaking pattern. A comparison of impact pressure on the cylinder was made by changing the cylinder to five different locations with respect to the breaking point. It was observed that the distance between the breaking point and the cylinder had a significant impact on the impact pressure on the cylinder. When the wave breaks directly in front of the cylinder, the greatest impact pressure on the cylinder occurs. The wave run-up due to the breaking wave hitting on the cylinder has significant effects on impact pressure acting on the vertical cylinder. For the same wave condition, the wave run-up and run-up pressure on the cylinder varied in five different test situations. The run-up near the breaking point was considerably higher than the run-up caused by other cylinder positions. Run-up pressure depends on the wave breaking pattern i.e., the run-up pressure is higher when the wave is just about to break, than when the wave has fully broken.

Acknowledgments

The authors appreciate the wave flume and experimental facilities provided by the Department of Ocean Engineering. The first author wishes to express his gratitude to the instrumentation team for their assistance during the trials.

References

Arntsen, Ø.A., Ros Collados, X. and Tørum, A. (2013), "Impact forces on a vertical pile from plunging breaking waves", *Proceedings of the Coastal Structures 2011*.

Büchmann, B., Skourup, J. and Cheung, KF. (1998), "Run-up on a structure due to second- order waves and a current in a numerical wave tank", *Appl. Ocean Res*., **20**(5), 297-308. https://doi.org/10.1016/S0141-1187(98)00022-4.

Chan, E.S. and Melville, W.K. (1989), "Plunging wave forces on surface-piercing structures", *J. Offshore Mech. Arct. Eng*., **111**(2), 92-100. https://doi.org/10.1115/1.3257093.

Chella, M.A., Bihs, H. and Myrhaug, D. (2019), "Wave impact pressure and kinematics due to breaking wave impingement on a monopole", *J. Fluid. Struct*., **86**, 94-123. https://doi.org/10.1016/j.jfluidstructs.2019.01.016.

Chellaa, M.A., Colladosc, X.R., Bihs, H., Myrhaugb, D. and Asgeir, Ø. (2016), "Numerical and experimental investigation of breaking wave", *Proceedings of the 13th Deep Sea Offshore Wind R&D Conference*, EERA DeepWind.

Esandi, J.M., Buldakov, E., Simons, R. and Stagonas, D. (2020), "An experimental study on wave forces on a vertical cylinder due to spilling breaking and near-breaking wavegroups", *Coast. Eng*., **162**, 103778. https://doi.org/10.1016/j.coastaleng.2020.103778.

Grue, J. and Osyka, B. (2021), "Runup on a vertical column in strong water wave events", *Coast. Eng*., **163**, 103775. https://doi.org/10.1016/j.coastaleng.2020.103775.

Ha, Y.J., Kim, K.H., Nam, B.W. and Hong, S.Y. (2020), "Experimental investigation for characteristics of wave impact loads on a vertical cylinder in breaking waves", *Ocean Eng*., **209**, 107470. https://doi.org/10.1016/j.oceaneng.2020.107470.

Hildebrandt, A. (2013), Hydrodynamics of breaking waves on offshore wind turbine structures, (Doctoral dissertation, Hannover: Gottfried Wilhelm Leibniz Universität Hannover).

Jian, W., Cao, D., Lo, E.Y., Huang, Z., Chen, X., Cheng, Z. and Li, B. (2017), "Wave runup on a surging vertical cylinder in regular waves", *Appl. Ocean Res*., **63**, 229-241. https://doi.org/10.1016/j.apor.2017.01.016.

Kamath, A., Chella, M.A., Bihs, H. and Arntsen, Ø.A. (2016), "Breaking wave interaction with a vertical cylinder and the effect of breaker location", *Ocean Eng*., **128**, 105-115. https://doi.org/10.1016/j.oceaneng.2016.10.025.

Kriebel, D.L. (1998), "Nonlinear wave interaction with a vertical circular cylinder: Wave forces", *Ocean Eng*., **25**(7), 597-605.

Kriebel, DL. (1992), "Nonlinear wave interaction with a vertical circular cylinder. Part II: Wave run-up", *Ocean Eng*., **19**(1), 75-99. https://doi.org/10.1016/0029-8018(92)90048-9.

Manjula, R., Sannasiraj, S.A. and Palanichamy, K. (2013), "Laboratory measurements of breaking wave impact pressures on a slender cylindrical member", *Int. J. Ocean Clim. Syst*., **4**, 151-169. https://doi.org/10.1260/1759-3131.4.3.151.

Mase, H., Kosho, K. and Nagahashi, S. (2001), "Wave runup of random waves on a small circular pier on a sloping seabed", *J. Waterw. Port Coast. Ocean Eng*., **127**(4), 192-199. https://doi.org/10.1061/(ASCE)0733-950X(2001)127:4(192).

Ochi, M.K. and Tsai, C.H. (1984), "Prediction of impact pressure induced by breaking waves on vertical cylinders in random seas", *Appl. Ocean Res*., **6**(3), 157-165. https://doi.org/10.1016/0141-1187(84)90005-1.

Oumeraci, H. (1994), "Review and analysis of vertical breakwater failures-lessons learned", *Coast. Eng*., **22**(1-2), 3-29. https://doi.org/10.1016/0378-3839(94)90046-9.

Sawaragi, T. and Nochino, M. (1984), "Impact forces of nearly breaking waves on a vertical circular cylinder", *Coast. Eng. Jap*., **27**, 249-263. https://doi.org/10.1080/05785634.1984.11924391.

Tanimoto, K., Takahashi, S., Kaneko, T. and Shiota, K. (1986), Impulsive pressure of breaking wave on piles, in: All Days. SPE, 492-496.

Vested, M.H., Carstensen, S. and Christensen, E.D. (2020), "Experimental study of wave kinematics and wave load distribution on a vertical circular cylinder", *Coast. Eng.*, **157**, 103660. https://doi.org/10.1016/j.coastaleng.2020.103660.

Wienke, J. and Oumeraci, H. (2005), "Breaking wave impact force on a vertical and inclined slender pile-theoretical and large-scale model investigations", *Coast. Eng.*, **52**(5), 435-462. https://doi.org/10.1016/j.coastaleng.2004.12.008.

Zhu, J., Gao, Y., Wang, L. and Li, W. (2022), "Experimental investigation of breaking regular and irregular waves slamming on an offshore monopile wind turbine", *Mar. Struct.*, **86**, 103270. https://doi.org/10.1016/j.marstruc.2022.103270.

RS